ELSEVIER

Catalysis Today 28 (1996) 431–441

CATALYSIS TODAY

Reaction of carboxylic acids on $CeO_2(111)$ and $CeO_2(100)$

J. Stubenrauch [a], E. Brosha [b], J.M. Vohs [a,*]

[a] *Department of Chemical Engineering and Laboratory for Research on the Structure of Matter, University of Pennsylvania, Philadelphia, PA 19104, USA*

[b] *Los Alamos National Laboratory, Los Alamos, NM 87545, USA*

Abstract

The reactions of HCOOH and CH_3COOH on $CeO_2(111)$ and $CeO_2(100)$ were studied using temperature programmed desorption (TPD) and high resolution electron energy loss spectroscopy (HREELS). The carboxylic acids were found to dissociate on both surfaces to form carboxylates. Adsorbed formates and acetates decomposed near 600 K to produce primarily the dehydration products CO and CH_2CO, respectively. This result is consistent with previous studies which have indicated that the ease of reduction of the oxide is the primary factor in determining the selectivity for dehydration versus dehydrogenation during carboxylate decomposition. In addition to CO and CO_2, small amounts of formaldehyde were produced during formate decomposition on both $CeO_2(111)$ and $CeO_2(100)$. In contrast, acetone was observed as a product during acetate decomposition only on the $CeO_2(111)$ surface.

1. Introduction

The selectivity for carboxylate dehydration versus dehydrogenation has long been used as a probe of the acid–base properties of metal oxide surfaces [1–4]. The conventional wisdom is that basic oxides exhibit a high selectivity for dehydrogenation, while acidic oxides favor dehydration. In recent years, however, studies of the decomposition of carboxylates on single crystal metal oxide surfaces suggest that this description may be somewhat oversimplified. For example, on MgO(100) formates decompose exclusively to CO in spite of the fact that MgO is considered to be highly basic [3]. On $SnO_2(110)$ two separate formate decomposition pathways have been observed, one which preferentially produces CO and one which preferentially produces CO_2 [5]. A similar result has also been reported for formate decomposition on $ZrO_2(100)$ [6]. In both of these cases, surface oxygen vacancies are thought to play an important role in determining reactivity. Based on these results as well as those obtained from TiO_2 surfaces, Barteau has suggested that the ease of reduction of the oxide is the principal factor in determining the relative amounts of CO and CO_2 produced during formate decomposition [3,7].

In addition to dehydration and dehydrogenation, bimolecular coupling of carboxylates has also been found to occur on metal oxide surfaces [7–9]. For example, on the {114}-faceted surface of $TiO_2(001)$ formates undergo a bimolecular reaction to produce formaldehyde,

* Corresponding author.

0920-5861/96/$32.00 Copyright © 1996 Elsevier Science B.V. All rights reserved.
PII S0920-5861(96)00251-9

while acetates react to form acetone [8]. Based on the fact that bimolecular coupling occurred only on surfaces that contained Ti cations with multiple coordination vacancies, it has been proposed that this reaction involves two carboxylates coordinated to a common surface Ti cation [7–9]. In addition to bimolecular coupling, it has also been reported that formaldehyde can be produced via a unimolecular reduction pathway. This appears to be the case for the reaction of formates on $SnO_2(110)$ [5].

In order to provide additional insight into the reaction pathways for carboxylates on metal oxide surfaces, in the present investigation we have studied the reaction of both formic and acetic acids on the (111) and (100) surfaces of CeO_2. Cerium dioxide has a fluorite crystal lattice. Schematic diagrams showing the ideal terminations for the (111) and (100) surfaces of this lattice are displayed in Fig. 1. The $CeO_2(111)$ surface has hexagonal symmetry and is formally composed of an outer layer of O^{-2} anions. The second layer of Ce^{+4} cations are also exposed on this surface. Both the cations and anions each have one vacancy in their respective coordination spheres relative to that in the bulk (i.e. they each have a single dangling bond). The $CeO_2(100)$ surface has fourfold symmetry and also has both cations and anions exposed. On this surface, however, the O^{-2} anions are fully coordinated, while the Ce^{+4} cations have four coordination vacancies.

2. Experimental

Experiments were conducted in two ultra-high-vacuum surface analysis systems. One system was primarily used for TPD experiments and contained a quadrupole mass spectrometer (UTI), a retarding field electron energy analyzer (Omicron), and an ion gun. The other chamber contained a high resolution electron energy loss spectrometer (McAllister), a cylindrical mirror analyzer (Omicron), and an ion gun. The base pressure in both chambers was maintained below 2×10^{-10} Torr.

The $CeO_2(111)$ single crystal wafer used in this investigation was approximately 7 mm × 4 mm × 1 mm in size and was cut from a larger crystal obtained from Commercial Crystal Laboratories. Prior to cutting, the crystal was oriented to expose the (111) surface using Laue x-ray diffraction. The (111) surface was polished until optically smooth by Commercial Crystal Laboratories using a proprietary method. The $CeO_2(100)$ substrate consisted of an epitaxial film of CeO_2 deposited on r-plane sapphire.

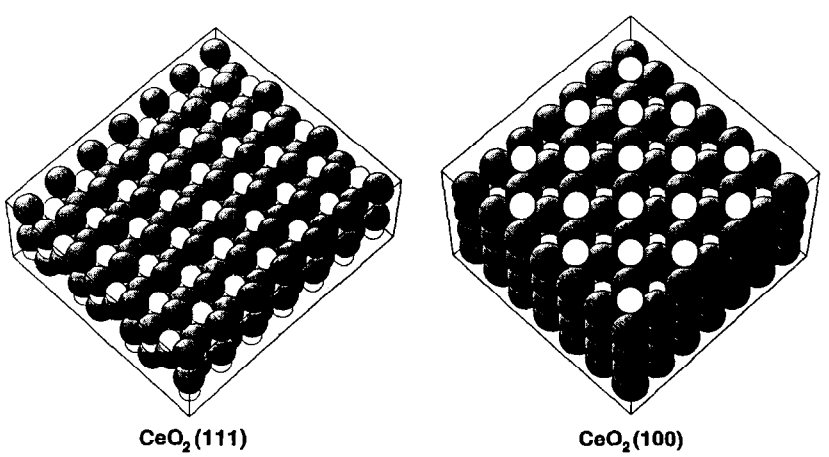

Fig. 1. Schematic diagrams of the ideal terminations of the $CeO_2(111)$ and $CeO_2(100)$ surfaces. The large shaded balls represent O^{-2} anions, while smaller unshaded balls represent Ce^{+4} cations.

The film was grown using 90° off axis RF magnetron sputtering with a gas phase consisting of 60% Ar and 40% O_2 at a total pressure of 4×10^{-2} Torr. The average thickness of the film was 100 Å and the orientation was verified using x-ray diffraction. AFM analysis of the surface of the film indicated that it was composed of crystalline domains with lateral dimensions of approximately 1000 Å × 1000 Å.

The $CeO_2(111)$ and $CeO_2(100)$ samples were mounted in tantalum holders which were attached to an UHV sample manipulator. The samples could be heated in excess of 950 K and cooled to 150 K via conduction from the sample holder. The temperature was monitored using a chromel–alumel thermocouple which was attached to the back face of the sample using a ceramic adhesive (Aremco #516).

Once in vacuum, the $CeO_2(111)$ sample was cleaned by sputtering with 500 eV Ar^+ ions for 30 min followed by annealing at 800 K in 1×10^{-7} Torr of O_2 for one hour. This sputter/anneal cycle was repeated until a clean, well ordered $CeO_2(111)$ surface was obtained as determined by AES and LEED. The $CeO_2(111)$ surface prepared in this manner exhibited a sharp hexagonal LEED pattern. Hexagonal symmetry is consistent with that expected for the ideal termination of this surface. The $CeO_2(100)$ epitaxial film was cleaned by annealing in 1×10^{-7} Torr of O_2 for one hour. The cleanliness of this surface was also monitored using AES. The insulating nature of the sapphire substrate precluded LEED analysis of this surface.

Formic acid (96% purity, Aldrich) and acetic acid (97% purity, Fisher Scientific) were vacuum distilled prior to use. Saturation exposures of the carboxylic acids were used in all experiments. TPD runs were performed with a heating rate of 3 K/s.

HREEL spectra were collected in the specular direction with an angle of incidence and reflection of 60° and an electron beam energy of 3.5 eV. The surface of the $CeO_2(100)$ film was apparently rather rough compared to that of the single crystal $CeO_2(111)$ surface and it was not possible to obtain high quality HREEL spectra from this sample. Therefore, HREELS results are reported only for $CeO_2(111)$. The $CeO_2(111)$ sample was maintained near 150 K during collection of HREEL spectra. For experiments in which the vibrational spectrum of an adsorbate was examined as a function of temperature, the sample was first heated to the desired temperature and then rapidly quenched to 150 K at which point an HREEL spectrum was collected.

Due to their limited conductivity, the CeO_2 samples used in this investigation became electrostaticly charged during irradiation with the low energy electrons. Thus, it was necessary to neutralize sample charging in order to collect HREEL spectra. This was done by irradiating the sample with a low flux of high energy electrons. Charge neutralization was achieved by balancing the flux of the incident high and low energy electrons with that of the emitted secondary electrons. This charge neutralization technique has been previously described in detail [10,11]. The high energy electron gun was operated with a beam energy of 400 eV and an emission current of approximately 10 uA.

The analysis of adsorbate features in the HREEL spectra of metal oxide surfaces is complicated by the presence of a series of intense losses due to multiple excitation of the dipole-active optical phonon modes of the oxide lattice [6,12–21]. In order to overcome this problem, the HREEL spectra were subjected to a Fourier deconvolution procedure which removed peaks due to multiple scattering events. This procedure has previously been described in detail [14,16,17] and applied in HREELS studies of adsorbates on ZnO(0001) [17,22], NiO(100) [21,23,24], MgO(100) [18], and $ZrO_2(100)$ [6]. An example of the application of this deconvolution procedure to the HREEL spectrum of clean $CeO_2(111)$ is displayed in Fig. 2. After deconvolution the phonon combination peaks which result from sequential scattering events are no longer present in the spectrum. Note that due to the limited signal-to-noise ratio in the raw data, small Fourier ripples were occasion-

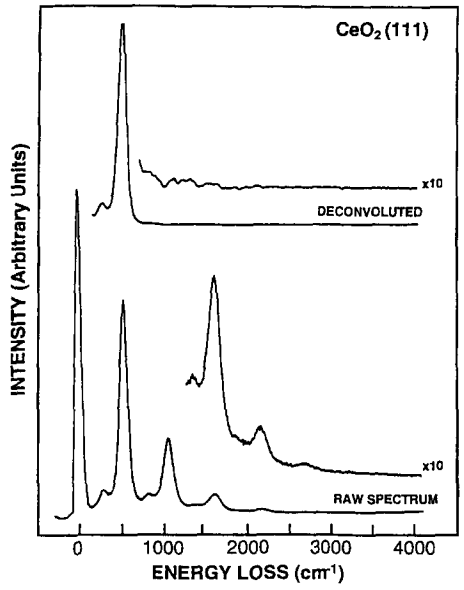

Fig. 2. HREEL spectrum of clean $CeO_2(111)$ before (lower portion) and after (upper portion) deconvolution.

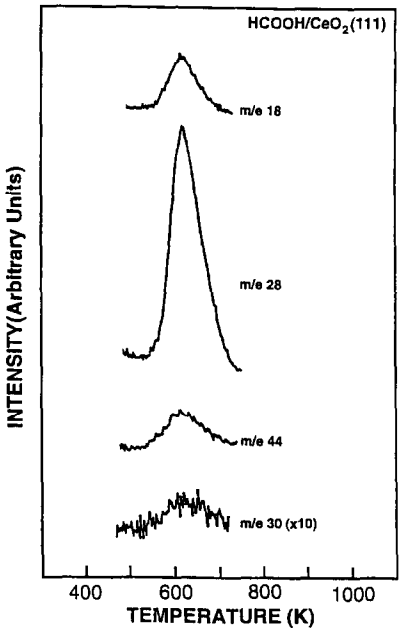

Fig. 3. TPD spectra obtained following exposure of $CeO_2(111)$ to 1 L of HCOOH. The m/e values of 30, 44, 28, and 18 correspond to H_2CO, CO_2, CO, and H_2O, respectively.

ally evident in the deconvoluted spectra. In order to assure that small adsorbate losses were correctly identified each HREEL experiment was repeated several times.

3. Results

3.1. Reaction of HCOOH and CH_3COOH on $CeO_2(111)$

Temperature programmed desorption spectra for the decomposition products obtained from HCOOH- and CH_3COOH-dosed $CeO_2(111)$ are displayed in Figs. 3 and 4, respectively. For the HCOOH-dosed surface, in addition to a small amount of molecular HCOOH which desorbed in a broad peak centered at 200 K, the only other products detected were CO ($m/e = 28$), CO_2 ($m/e = 44$), H_2O ($m/e = 18$), and CH_2O ($m/e = 30$), all of which desorbed at 610 K. The peak temperature for the decomposition products is similar to that which has been reported previously for reaction of formates on several other metal oxide surfaces, including

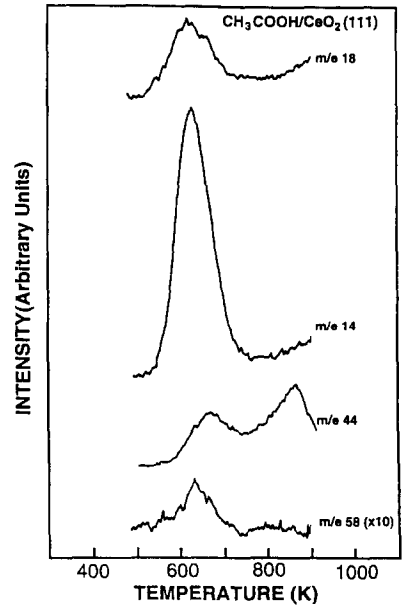

Fig. 4. TPD spectra obtained following exposure of $CeO_2(111)$ to 1 L of CH_3COOH. The m/e values of 58, 44, 14, and 18 correspond to $(CH_3)_2CO$, CO_2, CH_2CO, and H_2O, respectively.

Table 1
Product yields for formate decomposition

Desorption product	$CeO_2(111)$		$CeO_2(100)$	
	Yield fraction	Peak temp (K)	Yield fraction	Peak temp (K)
Carbon monoxide	1	610	1	650
Carbon dioxide	0.22	610	0.17	670
Water	0.32	610	0.40	650
Formaldehyde	0.05	610	0.04	650

$ZrO_2(100)$ [6], $SnO_2(110)$ [5], ZnO(0001) [25], and $TiO_2(001)$ [7]. Thus, for $CeO_2(111)$ these peaks can also be assigned to formate decomposition. The HREELS results presented below are consistent with this conclusion. As shown in Table 1, dehydration was highly favored over dehydrogenation during formate decomposition with the ratio of CO to CO_2 produced being 4.5. Formaldehyde accounted for less than 4% of the carbon-containing products.

TPD spectra for the decomposition products obtained from the CH_3COOH-dosed $CeO_2(111)$ are displayed in Fig. 4. The primary reaction pathway was again dehydration resulting in the production of ketene (CH_2CO, $m/e = 14$) at 635 K. Small amounts of acetone ($(CH_3)_2CO$, $m/e = 58$) and H_2O ($m/e = 18$) were also produced at this temperature, while CO_2 ($m/e = 44$) desorbed in two peaks centered at 860 and 680 K. The relative product yields, based on the TPD peak areas and measured cracking patterns, are listed in Table 2. In addition to the decomposition products shown in Fig. 4, molecular CH_3COOH was found to desorb in a broad peak between 180 and 300 K.

Table 2
Product yields for acetate decomposition

Desorption product	$CeO_2(111)$		$CeO_2(100)$	
	Yield fraction	Peak temp (K)	Yield fraction	Peak temp (K)
Ketene	1	635	1	680
Carbon dioxide	0.19	680	0.15	700
	0.16	860	0.05	780
Water	0.27	635	0.56	680
Acetone	0.06	635	0	–

The reactions of carboxylic acids on $CeO_2(111)$ were also studied using HREELS. Before presenting this data, the spectrum of the clean $CeO_2(111)$ surface will be briefly discussed. As shown in Fig. 2, the HREEL spectrum of $CeO_2(111)$ contains a series of intense losses which result from the excitation of the surface optical phonons (i.e. Fuchs–Kliewer phonons) of the lattice. The most prominent of these occurs at 550 cm^{-1}. This energy is consistent with that expected for the surface phonon mode based on the infrared optical constants of CeO_2 [26,27]. As noted above, multiple scattering events give rise to phonon–phonon combination peaks which occur at integer multiples of the phonon fundamental loss. The intensity of these combination losses follow that of a Poisson distribution. In addition to the surface phonon at 550 cm^{-1} a smaller loss is evident at 280 cm^{-1}. Peaks resulting from multiple excitations of this vibrational mode also appear throughout the spectrum. Although the intensity of this peak suggests that it is an additional phonon mode, a loss at this energy is not expected based on the bulk optical properties of CeO_2 [26,27]. Vibrational features in addition to those related to the bulk dielectric properties have also been observed in previous HREELS studies of ZnO(000T) [28] and LiF(100) [29]. In both of these cases it was postulated that the extra peaks resulted from excitation of vibrational modes localized at surface crystallographic defects. This explanation is reasonable in the case of $CeO_2(111)$ as well. Cerium cations are stable in both +3 and +4 oxidation states. As a result, CeO_2 can accommodate a high number of oxygen vacancies [30–33]. Thus, it would not be surprising if the surface contained a significant number of oxygen defects.

The HREEL spectrum of $CeO_2(111)$ dosed with 5 L of HCOOH at 180 K before and after deconvolution of the combination peaks is displayed in Fig. 5a. The deconvoluted spectrum contains adsorbate related features centered at 961, 1150, 1363, and 2885 cm^{-1}. Based on comparisons to the IR spectra of gaseous

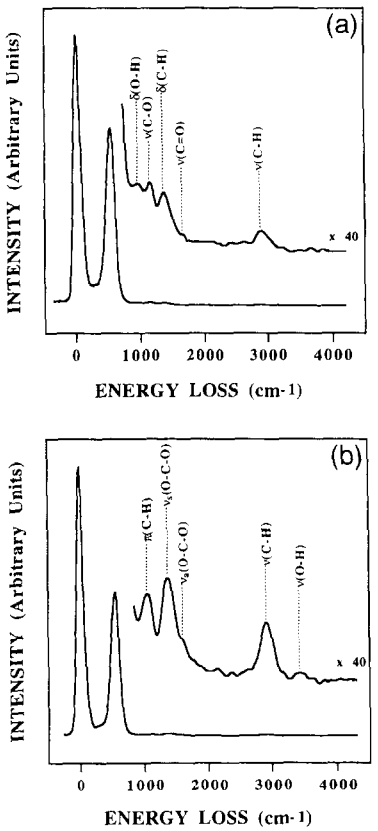

Fig. 5. HREEL spectrum of HCOOH-dosed $CeO_2(111)$: (a) following HCOOH adsorption at 180 K and (b) after heating the surface in (a) to 300 K.

HCOOH monomers and dimers [34], and to the HREEL spectra of HCOOH condensed on other metal oxides [6,17,20], these peaks can be assigned to the δ(O–H), ν(C–O), δ(C–H), and ν(C–H) modes of adsorbed formic acid, respectively. One would expect to observe the n(C=O) mode of formic acid near 1700 cm^{-1}. Although the HREEL spectrum does not contain a well-resolved peak at this location, there does appear to be a shoulder on the high-energy side of the δ(C–H) peak, which may be due to this mode. The presence of hydrogen bonding causes the O–H stretching mode of adsorbed HCOOH to be quite broad and difficult to detect in the HREEL spectrum of molecular HCOOH on metal oxide surfaces [6,20]. In the case of $CeO_2(111)$ this mode most likely overlaps with that of the C–H stretch. The position of the δ(O–H) peak, 961 cm^{-1}, is close to that reported for formic acid dimers in the gas phase [34]. This mode appears near 635 cm^{-1} in isolated formic acid molecules [34]. This suggests that at low temperature, HCOOH forms dimers on the $CeO_2(111)$ surface. A similar result has been reported for HCOOH adsorbed on $ZrO_2(100)$ [6] and NiO(100) [20].

Heating the HCOOH-dosed $CeO_2(111)$ surface to 300 K resulted in several changes in the HREEL spectrum relative to that obtained at low temperature. As shown in Fig. 5b, the spectrum at 300 K contains peaks due to adsorbates centered at 1040, 1370, 1590, 2880, and 3450 cm^{-1}. The peak at 3450 cm^{-1} is at an energy near that typically observed for the O–H stretching mode of hydroxyl groups on metal oxide surfaces [6,17,20,23,24]. The formation of surface hydroxyl groups indicates that the O–H group in adsorbed formic acid dissociates upon heating. The remaining peaks are in positions consistent with that of adsorbed formate species. The specific assignments for these peaks are

Table 3
Formate vibrational frequencies [a]

Vibrational mode	$CeO_2(111)$ HREELS	HCOONa IR [b]	ZnO(0001) HREELS [c]	$ZrO_2(100)$ HREELS [d]
π(C–H)	1055	1079	1079	1025
ν_s(O–C–O)	1370	1366	1387	1357
ν_a(O–C–O)	1590	1567	1612	1566
ν(C–H)	2880	2841	2939	2880

[a] All values are in cm^{-1}
[b] From Ref. [35]
[c] From Ref. [17]
[d] From Ref. [6]

listed in Table 3. The peak positions for formates adsorbed on ZnO(0001) [17] and ZrO_2(100) [6] as well as those for HCOONa [35] are also listed in this table for comparison.

The HREELS results for CH_3COOH-dosed CeO_2(111) were analogous to those obtained for HCOOH. At 150 K, the HREEL spectrum was consistent with that of molecular acetic acid. An HREEL spectrum obtained after dosing CH_3COOH at 150 K is displayed in Fig. 6a. By comparison to the IR spectrum of gaseous CH_3COOH [36] and the HREEL spectrum of CH_3COOH adsorbed on MgO(100) [18], the peaks centered at 913, 1030, 1390, 1700, and 2950 cm^{-1} can be assigned to γ(O–H), ν(C–C), ν(C–O) along with $\delta(CH_3)$, ν(C=O), and ν(C–H) modes, respectively. Once again the ν(O–H) mode is not resolvable and most likely contributes intensity to the ν(C–H) peak at 2950 cm^{-1}.

The most noticeable change in the HREEL spectrum of the CH_3COOH-dosed surface upon heating (see Fig. 6b) was the emergence of an O–H stretching mode at 3480 cm^{-1}, indicating dissociation of the adsorbed acetic acid to form acetate. The assignment of the acetate vibrational modes are listed in Table 4 as well as the peak positions for CH_3COONa and acetates adsorbed on NiO(100) [24] and MgO(100) [18].

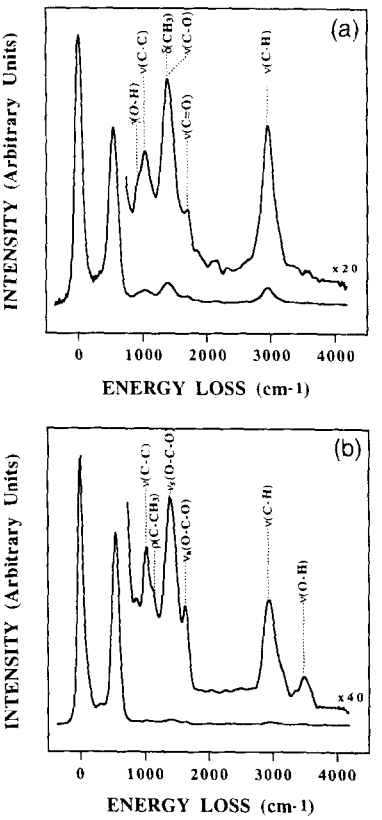

Fig. 6. HREEL spectrum of CH_3COOH-dosed CeO_2(111): (a) following CH_3COOH adsorption at 150 K and (b) after heating the surface in (a) to 300 K.

3.2. Reaction of $HCOOH$ and CH_3COOH on CeO_2(100)

Temperature programmed desorption spectra for the decomposition products obtained following a saturation dose of HCOOH on the CeO_2(100) surface are displayed in Fig. 7 and the relative product yields are listed in Table 1. With the exception of the peak temperatures, which are slightly higher, these spectra are

Table 4
Acetate vibrational frequencies [a]

Vibrational mode	CeO_2(111) HREELS	CH_3COONa IR [b]	NiO(100) HREELS [c]	MgO(100) HREELS [d]
ν(C–C)	1020	924	–	1000
$\rho(C–CH_3)$	1125	1012, 1043	–	–
δ(C–H)	–	1333, 1440	1302	–
ν_s(O–C–O)	1405	1421	1502	1449
ν_a(O–C–O)	1630	1583	1650	1579
ν(C–H)	2945	2955, 3000	3075	3066

[a] All values are in cm^{-1}
[b] From Ref. [35]
[c] From Ref. [24]
[d] From Ref. [18]

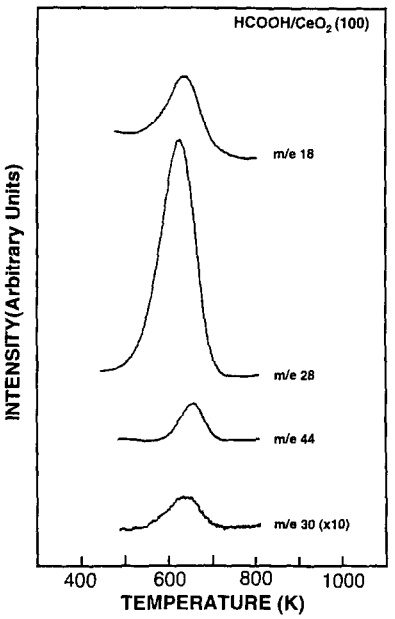

Fig. 7. TPD spectra obtained following exposure of $CeO_2(100)$ to 1 L of HCOOH. The m/e values of 30, 44, 28, and 18 correspond to H_2CO, CO_2, CO, and H_2O, respectively.

nearly identical to those obtained from the $CeO_2(111)$ surface. Thus, by comparison to the results obtained from the $CeO_2(111)$ surface the

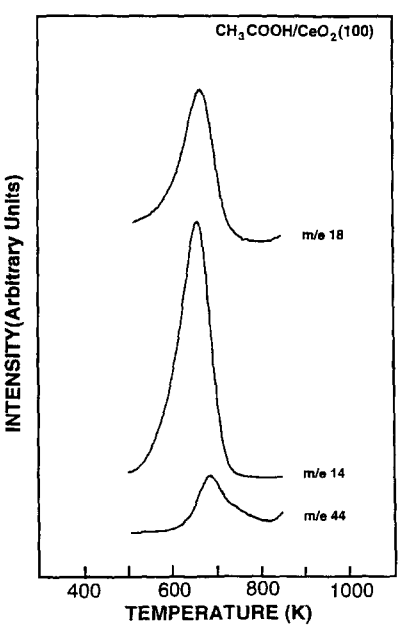

Fig. 8. TPD spectra obtained following exposure of $CeO_2(100)$ to 1 Langmuir of CH_3COOH. The mass-to-charge ratios of 44, 14, and 18 correspond to CO_2, CH_2CO, and H_2O, respectively.

products near 650 K can be assigned to decomposition of surface formate species.

The TPD results for the reaction of CH_3COOH on $CeO_2(100)$ were also similar to those obtained from $CeO_2(111)$. As shown in Fig. 8 and Table 2, the primary decomposition product was ketene which desorbed at 680 K. Water was also produced at this temperature. Carbon dioxide desorbed in two overlapping peaks centered at 700 and 780 K. The major difference between the TPD results obtained for the CH_3COOH-dosed $CeO_2(100)$ and $CeO_2(111)$ was the lack of acetone production on $CeO_2(100)$.

4. Discussion

The TPD and HREELS results demonstrate that HCOOH and CH_3COOH dissociate on $CeO_2(111)$ and $CeO_2(100)$ to form surface carboxylates and hydroxyl groups. Adsorbed formates are stable up to 600 K at which point they decompose producing CO and CO_2. The ratio of CO to CO_2 produced on $CeO_2(111)$ and $CeO_2(100)$ during formate decomposition was 4.5 and 5.9, respectively. Thus, on both surfaces dehydration was strongly favored over dehydrogenation. As noted above, it has been suggested that the ease of reduction of the oxide is related to the CO/CO_2 ratio during formate decomposition, with more easily reduced oxides producing more CO_2 [3,7]. Table 5 lists the CO/CO_2 ratios reported for formate decomposition on single crystal surfaces of several reducible oxides as well as the heat of formation for each oxide at 298 K. Comparison of the values in the table indicate that while surface structure has a minor influence on the CO/CO_2 ratio, there is a correlation between this ratio and the heat of formation of the oxide. Oxides which have a larger heat of formation exhibit a higher selectivity for the production of CO. This result provides further evidence that the reducibility of the oxide is an important factor in determining the selectivity for dehydration versus dehydro-

Table 5
CO/CO_2 for formate decomposition and $-\Delta H_f^o$ for various metal oxide surfaces

Metal oxide surface	CO/CO_2	$-\Delta H_f^o$ (kcal/mol) [f]
ZnO(0001)	0.26 [a]	84
TiO_2(001)-{114} faceted	2.1 [b]	125
TiO_2(001)-{011} faceted	2.8 [b]	
SnO_2(110)	2.5 [c]	142
CeO_2(111)	4.5 [d]	245
CeO_2(100)	5.9 [d]	
ZrO_2(100)	5.3 [e]	262

[a] From Ref. [25]
[b] From Ref. [7]
[c] From Ref. [5]
[d] From this study
[e] From Ref. [6]
[f] All values from Ref. [39]

genation during formate decomposition on metal oxides.

In addition to the oxidation products, a small amount of formaldehyde was also produced during formate decomposition. In previous studies of the reaction of formic acid on single crystal metal oxide surfaces, formaldehyde has been attributed to either a bimolecular reaction involving two formates [7,8] or to the reaction of formate with surface hydrogen [5]. Studies on faceted TiO_2(001) surfaces [7,8] indicate that the site requirement for the former pathway is a surface cation with at least two coordination vacancies. Multiple coordination vacancies are required in order to have two formate anions bound to a single surface cation. For CeO_2(100), the surface Ce cations meet this requirement and possess four coordination vacancies; however, the cations on the CeO_2(111) surface possess only a single coordination vacancy. The lack of multiple cation coordination vacancies on CeO_2(111) coupled with the fact that H_2CO is produced at the same temperature as the unimolecular decomposition products suggests that H_2CO is also a product of the unimolecular pathway. Apparently a portion of the hydrogen produced during formate decomposition can hydrogenate other formate species still on the surface. A similar pathway has been proposed to account for the production of H_2CO during formate decomposition on SnO_2(110) [5].

The primary decomposition pathway for acetate species on both CeO_2(111) and CeO_2(100) was also dehydration resulting in the production of ketene. In addition to ketene, small amounts of the complete oxidation product, CO_2, were also detected. For both surfaces, CO_2 was produced at two separate temperatures, the lower of which being close to the ketene desorption temperature. A similar two peak structure for CO_2 has been observed previously by Vohs and Barteau during acetate decomposition on ZnO(0001) [25]. In that study, based on XPS results, the low-temperature feature was assigned to non-selective decomposition of surface acetates, while the high-temperature feature was attributed to oxidation of surface carbon which was produced during the non-selective decomposition reaction. Since CO_2 was the only product produced at the higher temperature for the ceria surfaces, it is reasonable to also assign this feature to oxidation of surface carbon.

For the CH_3COOH-dosed CeO_2(111) surface a small amount of acetone was also detected. As noted above, for the {114}-faceted reconstruction of TiO_2(001) the production of acetone from surface acetates has been attributed to a bimolecular ketonization reaction involving acetates adsorbed on a common surface Ti^{+4} cation [8,9]. In the present case, however, acetone was produced only on the (111) surface suggesting that this product is not formed by an analogous pathway. If such were the case, one would expect a higher yield of acetone from the (100) surface on which the Ce cations have multiple coordination vacancies. The fact that acetone is produced at the same temperature as the dehydration products on the CeO_2(111) surface, suggests that it is simply a minor product of unimolecular decomposition. One possibility is that methyl groups, which are liberated during the non-selective acetate decomposition reaction, react with acetate species remaining on the surface to produce acetone. This pathway is

analogous to that proposed above for the production of formaldehyde from formates.

In addition to confirming the formation of surface formates and acetates, the HREELS results also provide some insight into the bonding configuration of these species on the $CeO_2(111)$ surface. Possible bonding configurations include monodentate in which only one of the oxygens in the carboxylate is bonded to a surface Ce^{+4} cation, symmetric bidentate in which both oxygens in the carboxylate are bonded to a single surface Ce^{+4} cation, and bridging in which each of the oxygens in the carboxylate are bonded to different surface Ce^{+4} cations.

It has previously been shown that the frequencies of the symmetric and asymmetric O–C–O stretching modes are sensitive to the carboxylate bonding configuration [23,37,38]. For example, based on comparisons between the IR spectra of a wide variety of acetate complexes of known structure, Deacon and Phillips have proposed a correlation between the difference in the frequencies of the ν_a(OCO) and ν_s(OCO) modes, D, and the acetate bonding configuration [38]. They report that values of D that are significantly greater than 200 cm^{-1} result exclusively from monodentate coordination, while values less than 100 cm^{-1} are usually due to bidentate bonding. Intermediate values of D (i.e. $100 < 200$) are more difficult to assign and can be due to either bidentate or bridging acetates. These general guidelines have been used previously to assign the bonding configuration of acetates adsorbed on hydroxylated NiO(111) thin films [23]. For acetates on $CeO_2(111)$ the value of D was 225 cm^{-1}, indicating a monodentate configuration for acetates on this surface.

A monodentate bonding configuration is consistent with what would be predicted based on the structure of the $CeO_2(111)$ surface. Since the cations on this surface have only a single coordination vacancy, bidentate bonding is unlikely. Moreover, the distance between cerium nearest neighbors on $CeO_2(111)$ is 3.83 Å, a value significantly greater than the oxygen–oxygen distance in sodium acetate (2.2 Å). Thus, bonding in a bridging configuration also appears to be improbable.

By analogy to the results for acetates, formates would also be expected to bond in a monodentate configuration on the $CeO_2(111)$ surface. The HREELS results are consistent with this conclusion. The D value for formates on $CeO_2(111)$, 220 cm^{-1}, is close to that obtained for acetates. Monodentate formate species on ZnO(0001) [17] have a similar D value of 225 cm^{-1}.

Since HREEL spectra could not be obtained from the $CeO_2(100)$ sample, we can only speculate about the bonding configuration for carboxylates on this surface. Assuming that $CeO_2(100)$ does not undergo any major reconstructions, the bridging configuration can again be excluded based on the large separation of the surface cations. Unlike $CeO_2(111)$, however, the cations on $CeO_2(100)$ are likely to have multiple coordination vacancies. Thus, it may be possible to form either monodentate or bidentate species on this surface. Since both CeO_2 and ZrO_2 have the same fluorite structure, a recent study of the bonding of formates on $ZrO_2(100)$ [6] may provide some insight into the interaction of carboxylates with $CeO_2(100)$. For $ZrO_2(100)$, HREELS results indicated a symmetric bidentate configuration for adsorbed formates. Thus, a similar configuration would be expected on $CeO_2(100)$.

5. Conclusions

Formic and acetic acids were found to dissociate on both the $CeO_2(111)$ and $CeO_2(100)$ surfaces to form formate and acetate intermediates. At 610 K, formates decomposed to produce primarily CO and H_2O. Small amounts of CO_2 and H_2CO were also produced at this temperature. The primary pathway for acetate decomposition was again dehydration to produce CH_2CO and H_2O. Small amounts of CO_2 were detected during acetate decomposition on both CeO_2 surfaces, while $(CH_3)_2CO$ was pro-

duced only on the $CeO_2(111)$ surface. The ratio of CO to CO_2 produced during formate decomposition on CeO_2 along with those reported for other single crystal oxide surfaces, indicates that this ratio correlates with the heat of formation of the oxide. The HREELS results obtained from $CeO_2(111)$ indicate that both formates and acetates bond to this surface in a monodentate configuration.

Acknowledgements

We gratefully acknowledge the Laboratory for the Structure of Matter at the University of Pennsylvania for the use of their facilities as well as the National Science Foundation for support of this research through the NSF-MRL program (grant # DMR91-20668). We would also like to thank R. Houlton for his assistance in preparing the $CeO_2(100)$ film.

References

[1] M. Ai, J. Catal., 50 (1977) 291.
[2] P. Mars, J.J.F. Scholten and P. Zwietering, Adv. Catal., 14 (1963) 35.
[3] X.D. Peng and M.A. Barteau, Cat. Lett., 7 (1990) 395.
[4] X.D. Peng and M.A. Barteau, Langmuir, 7 (1991) 1426.
[5] V.A. Gercher and D.F. Cox, Surf. Sci., 312 (1994) 106.
[6] P.A. Dilara and J.M. Vohs, J. Phys. Chem., 97 (1993) 12919.
[7] K.S. Kim and M.A. Barteau, Langmuir, 6 (1990) 1485.
[8] K.S. Kim and M.A. Barteau, Langmuir, 4 (1988) 945.
[9] K.S. Kim and M.A. Barteau, J. Catal., 125 (1990) 353.
[10] P.A. Thiry, M. Liehr, J.J. Pireaux, R. Sporken, R. Caudano, J.P. Vigneron and A.A. Lucas, J. Vac. Sci. Technol., 3 (1985) 1118.
[11] P.A. Thiry, M. Liehr, J.J. Pireaux and R. Caudano, J. Electron Spectrosc. Relat. Phenom., 39 (1986) 69.
[12] K.L. D'Amico, F.R. McFeely and E.I. Solomon, J. Am. Chem. Soc., 105 (1983) 6380.
[13] P.A. Cox, R.G. Egdell and P.D. Naylor, J. Electron Spectrosc. Relat. Phenom., 29 (1983) 247.
[14] P.A. Cox, W.R. Flavell, A.A. Williams and R.G. Egdell, Surf. Sci., 152/153 (1985) 784.
[15] H. Ibach and D.L. Mills, Electron Energy Loss Spectroscopy and Surface Vibrations, Academic Press, New York, 1982.
[16] R.G. Egdell, in M. Che and C.C. Bond (Editors): Adsorption and Catalysis on Oxide Surfaces, Elsevier, Amsterdam, 1985, p. 173.
[17] W.T. Petrie and J.M. Vohs, Surf. Sci., 245 (1991) 315.
[18] W.T. Petrie and J.M. Vohs, Surf. Sci. Lett., 259 (1991) L750.
[19] G. Rocker, J.A. Schaefer and W. Gopel, Phys. Rev. B, 30 (1984) 3704.
[20] C.M. Truong, M. Wu and D.W. Goodman, J. Phys. Chem., 97 (1992) 9447.
[21] K.W. Wulser and M.A. Langell, J. Electron Spectrosc. Relat. Phenom., 59 (1992) 223.
[22] W.T. Petrie and J.M. Vohs, J. Vac. Sci. Technol., 11 (1993) 2169.
[23] M.A. Langell, C.L. Berrie, M.H. Nassir and K.W. Wulser, Surf. Sci., 320 (1994) 25.
[24] K.W. Wulser and M.A. Langell, Catal. Lett., 15 (1992) 39.
[25] J.M. Vohs and M.A. Barteau, Surf. Sci., 201 (1988) 481.
[26] F. Marabelli and P. Wachter, Phys. Rev. B, 36 (1987) 1238.
[27] S. Mochizuki, Phys. Stat. Sol., 114 (1982) 189.
[28] W.T. Petrie and J.M. Vohs, J. Chem. Phys., 101 (1994) 8098.
[29] J.J. Pireaux, P.A. Thiry and R. Caudano, Surf. Sci., 162 (1985) 132.
[30] M. Breysse, M. Guenin, B. Claudel, H. Latreille and J. Veron, J. Catal., 27 (1972) 275.
[31] D.A. Creaser, P.G. Harrison, M.A. Morris and B.A. Wolfindale, Catal. Lett., 23 (1994) 13.
[32] M. Mogensen, J. Electrochem. Soc., 139 (1992) 577.
[33] T.X.T. Sayle, S.C. Parker and C.R.A. Catlow, Surf. Sci., 316 (1994) 329.
[34] R.C. Millikan and K.S. Pitzer, J. Am. Chem. Soc., 80 (1958) 3515.
[35] E. Spinner, J. Chem. Soc., (1964) 4217.
[36] K. Ito and H.J. Bernstein, Can. J. Chem., 34 (1956) 170.
[37] B.A. Sexton and R.J. Madix, Surf. Sci., 105 (1981) 177.
[38] G.B. Deacon and R.J. Phillips, Coord. Chem. Rev., 33 (1980) 227.
[39] R.C. Weast, M.J. Astle and W.H. Beyer, Handbook of Chemistry and Physics, 67th ed., CRC Press, Boca Raton, FL, 1986–87, p. D-33.